Journal of the European Ceramic Society 22 (2002) 209–218

www.elsevier.com/locate/jeurceramsoc

Experimental and theoretical study of the ferroelectric and piezoelectric behavior of strontium-doped PZT

R.S. Nasar[a,*], M. Cerqueira[a], E. Longo[b], J.A. Varela[c], A. Beltran[d]

[a]*Departamento de Química, UFRN, Caixa postal 1662, CEP 59072-970 Natal-RN, Brazil*
[b]*Laboratório Interdisciplinar de Eletroqulmica e Cerâmicas, Departamento de Química, UFSCar, Caixa Postal 676, CEP 13565-905 São Carlos-SP, Brazil*
[c]*Instituto de Química, UNESP, Caixa Postal 355, CEP 14800-900 Araraquara-SP, Brazil*
[d]*Departament de Ciencies Experimentals, Universitat Jaume I, PO Box 242, 12080 Castelló, Spain*

Received 17 August 2000; received in revised form 7 February 2001; accepted 16 February 2001

Abstract

Theoretical data using ab initio perturbed ion calculation were compared with ferroelectric and piezoelectric experimental data of strontium doped PZT. Various concentrations of SrO in PZT at constant temperature and sintering time were carried out. Experimental results, such as the remanent polarization, $\mathbf{P_R}$ of 6.9–8.9 μC/Cm^2, the coercive field, $\mathbf{E_C}$ of 6.6–7.8 kVcm, and the planar coupling factor, **Kp** of 0.45–0.53, were compared with the energy of Zr^{4+} and Ti^{4+} ion dislocation and the lattice interaction energy which show that strontium increment in PZT alter the energies and increase the values of piezoelectric and ferroelectric variables. Calculations of lattice energy of the rhombohedral phase show that a phase non-stability is coincident with increasing experimental values of the $\mathbf{P_R}$, $\mathbf{E_C}$ and **Kp**.

Keywords: Calculations-aiPI; Ferroelectrics; Piezoelectrics; PZT

1. Introduction

A solid solution of $PbZrO_3$–$PbTiO_3$ (PZT, lead zirconate titanate) has ferroelectric properties and its polarization presents piezoelectric response with important technological applications.[1–7] This non-centrosymmetric material of ABO_3 perovskite type structure has a ferroelectric tetragonal phase, $\mathbf{F_T}$ (titanium rich region), ferroelectric rhombohedral phase, $\mathbf{F_R}$ (zirconium rich region) and ferroelectric orthorhombic phase, $\mathbf{F_O}$ (small titanium concentration). Higher than Curie temperature it has paraelectric cubic phase, Pc. It is know that ferroelectric properties result from displacive transition[8] of Zr^{4+}/Ti^{4+} ions between two stable off-centered sites of Ti06.Zr06 octaédra due to an external field.

According to some authors[9,10] moisture of stoichiometric ratio of ZrO_2/TiO_2, mol% from 0.52/0.48 to 0.55/0.45 leads to a compositional fluctuation with tetragonal and rhombohedral phase coexistence observed in the phase diagram. However, other authors[11–13] consider that the use of the wet processing method will lead to only one phase near to that region. Such regions have excellent piezoelectric properties and are denominated by morphotropic phase boundary (MPB).[13,14]

Factors, such as physico-chemical characteristics of precursors, additive type and processing alter the ferroelectric and piezoelectric properties of this material.

Phase's type and microstructure characteristics cause modification of factors, such as, remnant polarization, $\mathbf{P_R}$, coercive field, $\mathbf{E_C}$ and the planar coupling factor, $\mathbf{K_P}$. Experimental studies of Zhang et al.[15] show that piezoelectric and dielectric property transformation below 300 K occurs due to the activity change of domain walls in the material. As a complement, Bernard[16] and Kulcsar[17] that Pb^{2+} replaced Sr^{2+} and that Ca^{2+} in the lattice increases the $\mathbf{K_p}$ value.

Comparisons between theoretical and experimental data studied by Cerqueira et al.[18] and Nasar et al.[19] that used a replacement of A^{+2} position by Ca^{2+} and Ba^{2+}, respectively in the ABO_3 perovskite structure show high conformity of theoretical data of the crystalline lattice energy and the potential barrier due to Zr^{4+} and Ti^{4+}

* Corresponding author. Tel.: +55-084-215-3823; fax: +55-084-211-9224.
E-mail address: nasar@zaz.com.br (R.S. Nasar).

0955-2219/01/$ - see front matter
PII: S0955-2219(01)00256-4

ion dislocation in the structure with experimental values of $\mathbf{P_R}$, $\mathbf{E_C}$ and $\mathbf{K_P}$.

Jaffe et al.[20] considered that, as a phase influence, the tetragonal structure favors the piezoelectric properties in opposition to the effect caused by a rhombohedral structure. However, Galasso[21] proposed that the tetragonal phase consists of displacement along four cube diagonals giving an average structure with a polarization along [100] while the rhombohedral phase is ordered along [111].

For comprehension of the physical and chemical properties of ferroelectric and piezoelectric materials a study is presented of combined experimental and theoretical approach to piezoelectric behavior of PZT, doped with Sr^{2+}. The experimental part consists of a systematic study of influence of various Sr^{2+} concentrations (from 0.25 to 1.5 mol%) in PZT at constant temperature and sintering time.

A comparative study of ferroelectric and piezoelectric characteristics, such as, remnant polarization, $\mathbf{P_R}$, coercive field, $\mathbf{E_C}$ and the planar coupling factor, $\mathbf{K_P}$ are done. An initial perturbed ion (aiPI) calculation, as a theoretical methodology was used and data of lattice energy and the potential barrier energy of Zr^{4+} and Ti^{4+} ion dislocation in the tetragonal and rhombohedral structure are analysed and compared with experimental results.

2. Experimental procedure

2.1. Synthesis

High purity raw materials, such as $Pb(NO_3)_2$ (99.7%, Merck); ZrO_2 (99.7%, Merck); TiO_2 (99.2%, Aldrich); $Sr(CH_3–COO)_2$ (99.2%, Reagen) were used. Powder of compositions $(Zr_{0.53}Ti_{0.47})O_2$ (ZT) was prepared by mixing and grinding zirconia and titania powders for 24 h in isopropyl alcohol medium. Solid state reaction by calcination at 1450°C for 2 h was carried out.

The ZT (53/47) phase was suspended in water while stirring and adding lead nitrate for building a Pb $(Zr_{0.53}Ti_{0.47})O_3$ composition in this solution. $Pb(OH)_2$ was precipitated onto ZT particles by addition of NH_4OH until reaching the value of pH 11. The mass precipitated was washed, filtered and dried at a temperature of about 60°C.

Strontium acetate was precipitated onto ZT particles with $Pb(OH)_2$ in isopropyl alcohol medium. After precipitation the solution was stirred for 2 h and then dried, deagglomerated in a mortar and granulated in a 200-mesh screen. From 0.25 to 1.50 mass% of strontium oxide were added in different batches and the powder mixture was calcined at 850°C for 2 h and the phases were analyzed by the Rietveld method.[22] Samples with 2 g of weight and 2 cm diameter were pressed isostatically with 150 MPa and sintered at atmosphere at 1150°C for 3 h.

2.2. Characterization

The ZT powder was deagglomerated in an alumina mortar and characterized by using X-ray diffractometry, (XRD; Siemens Model D-5000). The PZT powder was characterized by XRD with the use of the Rietveld method.

2.2.1. Rietveld method

A comparison was carried out between a calculated X-ray diffraction pattern, with defined crystallographic parameters, and an experimental pattern by using the Rietveld method. A scanning process "step by step" with constant increment and time obtained experimental peaks.

A peak definition is a total contribution of different factors, such as: structure factor, multiplicity factor, Lorentz factor, scale factor and others.

At the multiphase the following was analysed:

$$Yec = S\sum_{h} L_h |F|_h^2 G(\Delta\theta) P\kappa + Ybi \quad (1)$$

S = scale factor.

F = The structure factor of (h, k, l) plane that has 1, 2, 3, ... n atoms,

Respectively at positions $U1$, $V1$, $W1$; $U2$, $V2$, $W2$; Un, Vn, Wn is obtained by:

$$Fhkl = \sum_{1}^{n} f_n e^{2\pi(hUn+kVn+lWn)}$$

Where $f_1, f_2 \ldots f_n$ is the atomic scattering factors and is on θ and λ functions.

G = The reflection profile function which approximates the effects of both instrumental and, possibly, specimen features.

Pk = The preferred orientation function, here implemented both (operators choice), (a) as $(G2+(1-G2)*\exp(G1\alpha^2 k))$, Toraya' s modification of the function used in the original Rietveld program, and (b) as $(G^2 1\cos^2\alpha + (1/G1)\sin^2\alpha)^{-3/2}$, the March–Dollase function, where $G1$ and $G2$ are refinable parameters and αk is the angle between d^*k and the presumed cylindrical — symmetry axis of the texture (e.g. fiber axis direction).

L_h = Lorentz, polarization factor and multiplicity factors. The multiplicity factor considers a scattering bean consider a relative proportion of planes contributing to the reflexion. It is defined by a number of planes with the same d displacement. Parallel planes are separated counted. A cubic crystal has a multiplicity factor of 6 for {001} planes and 8 for {111} planes. The Lorentz

and polarization factors consider a scattering bean of an electron, where $PF=(1+\cos^2 2\theta)/2$ and trigonometric factors where $LF=[1/(4\sin^2\theta\cos\theta)]$. The total effect of these geometric factors described the reflections of intensity that occurs at intermediary angles.

$\Delta\theta=\theta$ angle *i*th,
Ybi = next peak contributions.

An approximation between the observed X-ray diffraction pattern and the calculations was made, by least squares using the Gaussian curve type.

New refined parameters were obtained from the calculated X-ray diffraction profile. Both, the refined profile and the phase's deconvolution were obtained from the peaks of the X-ray diffraction pattern.

2.2.2. Scanning electron microscopy (SEM)

An energetic electron beam interacted with the sample surface (~1.5 μm) and caused scattering of electrons, XRF (X-ray fluorescence), XRD (X-ray diffraction) and others. Electron detectors switched electric signal for a cathodic ray tube (CRT) and produced contrast and an energetic surface image is obtained by different positions of electron emission relative to the sample — detector system. Both polished and fracture surface could be analyzed independently of focus distance to the superficial imperfections. Porosity, microstructure homogeneity and grain sizes of sintered powder were observed using a Jeol JSM-T 330A.

3. Theoretical method and models

3.1. Method

The theory of electronic separability[23,24] demonstrated that a system can be partitioned into weakly interacting groups, the electronic wave function of the system can be written as an antisymmetrized product of wave functions. If ψ_A is the wave function of a relevant group, for example, the active (**A**) group, whose self-consistent field (SCF) equations are solved in the field of the remaining (frozen) groups, the contributions of **A** to the total energy can be collected in the effective energy

$$E^A_{\text{eff}} = E^A_{\text{net}} + \sum_{R(\neq A)} E^{AR}_{\text{int}} = E^A_{\text{net}} + E^A_{\text{int}} \tag{2}$$

R = any group different of the **A** group that interact with **A**

Which gives, by minimization, the best ψ_A for a set of given frozen groups.

The effective energy arises from the contribution of internal energy of the group, E_{net}, and the interaction energy, E_{int} for this group with each of the ions in the lattice.

The total energy of the system is not the sum of the group effective energies. However, we can define the additive energy of the A group as

$$E^A_{\text{add}} = E^A_{\text{net}} + \frac{1}{2}E^A_{\text{int}} \tag{3}$$

For an, as example, *AaBbOc*... ionic crystal, the ions (A, B, O, ...) are stabilized by ion-lattice interaction energy, and the crystal energy per molecule is:

$$\begin{aligned} E_{\text{cryst}} &= aE^A_{\text{add}} + bE^B_{\text{add}} + cE^O_{\text{add}} \ldots \\ &= aE^A_{\text{net}} + bE^A_{\text{net}} + cE^A_{\text{net}} \ldots + \frac{1}{2} \\ &\quad \times \left(aE^A_{\text{net}} + bE^B_{\text{int}} + cE^O_{\text{int}} \ldots\right) \end{aligned} \tag{4}$$

The lattice energy (E_{latt}) in the aiPI method is given by,

$$E_{\text{latt}} = E_{\text{cryst}} - \left(aE^A_0 + bE^B_0 + cE^O_0 + \ldots\right) \tag{5}$$

Where the subscripted 0 stands for "free-ion values".

3.2. Basis set representation

A large STO (slater type orbital) basis set was used on each atomic center 7s5p on Sr^{2+} and Ti^{4+}, 5s5p on O^{2-}, 10s9p5d on Zr^{4+}[25] and 12s8p6d2f on Pb^{2+}[26]. An optimization of these basis sets was done in order to minimize the total energy while maintaining SCF stability.

A case for interaction between orbitals of two atoms,

$\Psi(1,2) = 1/1.34!$ multiplying the matrix

$$\begin{vmatrix} \Psi\alpha(1) & \Psi\alpha(1) \\ \Psi\alpha(2) & \Psi\alpha(2) \end{vmatrix}$$

A slater determinant could be used. The general algebric properties of determinants imply that expressions change sign when any two variables are exchanged and vanish when any two spin-orbital indices denote the same state. Consequently, slater determinants automatically satisfy the Pauli principle and furnish the basic solutions for use in the Hartree–Fock self-consistent procedure.[25]

Contributions of quantum mechanical energy to the interaction energies was considered for a large number of neighboring shells up to attaining a convergence of 10–6 Hartrees in the crystal energy. The Madelung potential, responsible for the largest part of the interaction energies was integrated analytically. Layer by layer Ewald summation techniques were used, accurately to sum up long-range Coulomb potential contributions.

An optimization of theoretical data of PZT structure (energies) was carried out by varying the Ti^{4+}/Zr^{4+} z-fractional coordinate by means of rhombohedral (space group R $\bar{3}$ m) (Zr^{4+} in B position) and tetragonal (space group P $\bar{4}$ mm) (Ti^{4+} in B position) structures. They have been maintained the experimental values obtained from X-ray diffraction experiments of the parameters for pure and doped PZT, such as, lattice and positional parameters, by using the Rietveld method.

The polarization parameters were defined as a measure of lattice stability, ϵE the minimum lattice displacement energy (0 Å) is $E_{m,\ T,\ R}$ and the maximum lattice displacement energy (0.05 Å) is $E_{M,\ T,\ R}$ for both tetragonal and rhombohedral structures.

$$\Delta E = E_{m,\ T,\ R} - E_{M,\ T,\ R} \quad (6)$$

For the initial calculation an "infinity's crystal was considered, e. g.: PZT(0.53 $PbZrO_3$/0.47 $PbTiO_3$). In the following, for representation of the doping contribution in the structure, alleatory substitutions in this infinity crystal were carried out. Substitutions were carried out, such as barium at the position of lead with the same initial stoichiometry (see Table 1).

4. Results and discussion

4.1. Phase analysis of powder

Fig. 1a shows the analysis of calcined powder by X-ray diffraction pattern, XRD of different strontium concentrations in PZT (53/47). Occurrence of coexistence between tetragonal, (F_T) and rhombohedral, (F_R) phases (Fig. 1b) was observed. There exists controversy between authors: according to Kakegawa et al.[26] the use of a wet method leads to a monophasic PZT in the MPB region so that, an F_T phase occurs when $x = 0.53$, and above this Zr concentration, an F_R phase is stable. However, authors such as Isopov[11,13] demonstrated that the dry method causes a phase coexistence for both tetragonal and rhombohedral phase, between $0.52 \geqslant x \geqslant 0.54$ of Zr concentration in the MPB region.

A phase analysis (Fig. 2 and the quantity phase analysis of calcined PZT), by peak deconvolution, shows that only an F_T occurs (Table 2), the same results were obtained by Kakegawa et al.[26] that showed an F_T phase. The increase of the F_R phase shows that additions of strontium promoted a dislocation from tetragonal ferroelectric, ($\mathbf{F_T}$), PZT to tetragonal and rhombohedral ferroelectric ($\mathbf{F_{T,\ R}}$) phases (MPB), Sr-PZT in the phases diagram. Such phase's alteration occurs due to a solid state formation with an Sr^{2+} replaced by Pb^{2+} (solid solution) in the perovskite structure without vacancy creation. A coexistence of phases occurs due to a compositional fluctuation (different chemistry potential caused by non-homogeneity) of Zr^{4+} and Ti^{4+} ions in the PZT structure.[26] The same results were obtained when the using calcium[18] and barium oxide[19] doped PZT. Lattice parameter variation was observed with a decrease of $(\mathbf{c}/\mathbf{a})_T$ and a small a_R parameter alteration.

Deconvolution of diffraction peaks of strontium doped PZT (Table 3) shows a decrease of F_T phase due to an appearance of F_R phase of Sr-PZT. The systematic addition of SrO shows the formation of rhombohedral phase caused by an increase of compositional fluctuation with a consequent coexistence of F_T and F_R phases. Such substitutions of Sr^{2+} replaced by Pb^{2+} caused a solid solution formation with a strong decrease of $(c/a)_T$ relation due to a minor repulsion between the Sr^{2+} and O^{2-} orbitals in the structure. This phenomena favors a c-direction approximation in the unit cell with a consequent alteration of dipole formation due to a minor Zr^{4+}/Ti^{4+} ion dislocation. The tensioned rhombohedral structure, that is a modification of a cubic structure, does not have substantial alteration due to a likely deformation (stretching) of chemical bonding in the structure. A small optimization effect of the sintering process was observed by SrO concentration with a consequent increase of the apparent density.

4.2. Theoretical study and comparison with experimental data

Theoretical analysis (Fig. 3) of the lattice energy, for different SrO concentrations in PZT, shows a high sta-

Table 1
Stoichiometric composition of a cluster of the PZT phase for theoretical calculations

PZT		$SrZrO_3$(SrZ)/$SrTiO_3$ (SrT)
0.00 Sr- PZT	0.53$PbZrO_3$(PZ)/0.47$PbTiO_3$(PT)	
0.25 Sr- PZT	(0.53–0.0125)PZ/(0.47–0.0125)PT	0.0125SrZ/0.0125 SrT
0.50 Sr- PZT	(0.53–0.025)PZ/(0.47–0.025)PT	0.025 SrZ/0.025 SrT
1.00 Sr- PZT	(0.53–0.05)PZ/(0.47–0.05)PT	0.05 SrZ/0.05 SrT
1.50 Sr-PZT	(0.53–0.075)PZ/(0.47–0.075)PT	0.075 SrZ/0.075 SrT

The final composition of doped PZT = $_{(0.5175PZ+0.0125SrZ)}$ + $_{(0.4575PT+0.0125SrT)=0.25Sr\text{-}PZT(53/47)}$. A cluster with 300 unit cells of ABO_3 structure, close to 155 unit cells (51.75%) has Zr in B positions, 137 unit cells (45.75%) has Ti in B positions and 8 unit cells (2.5%) has Sr in A positions.

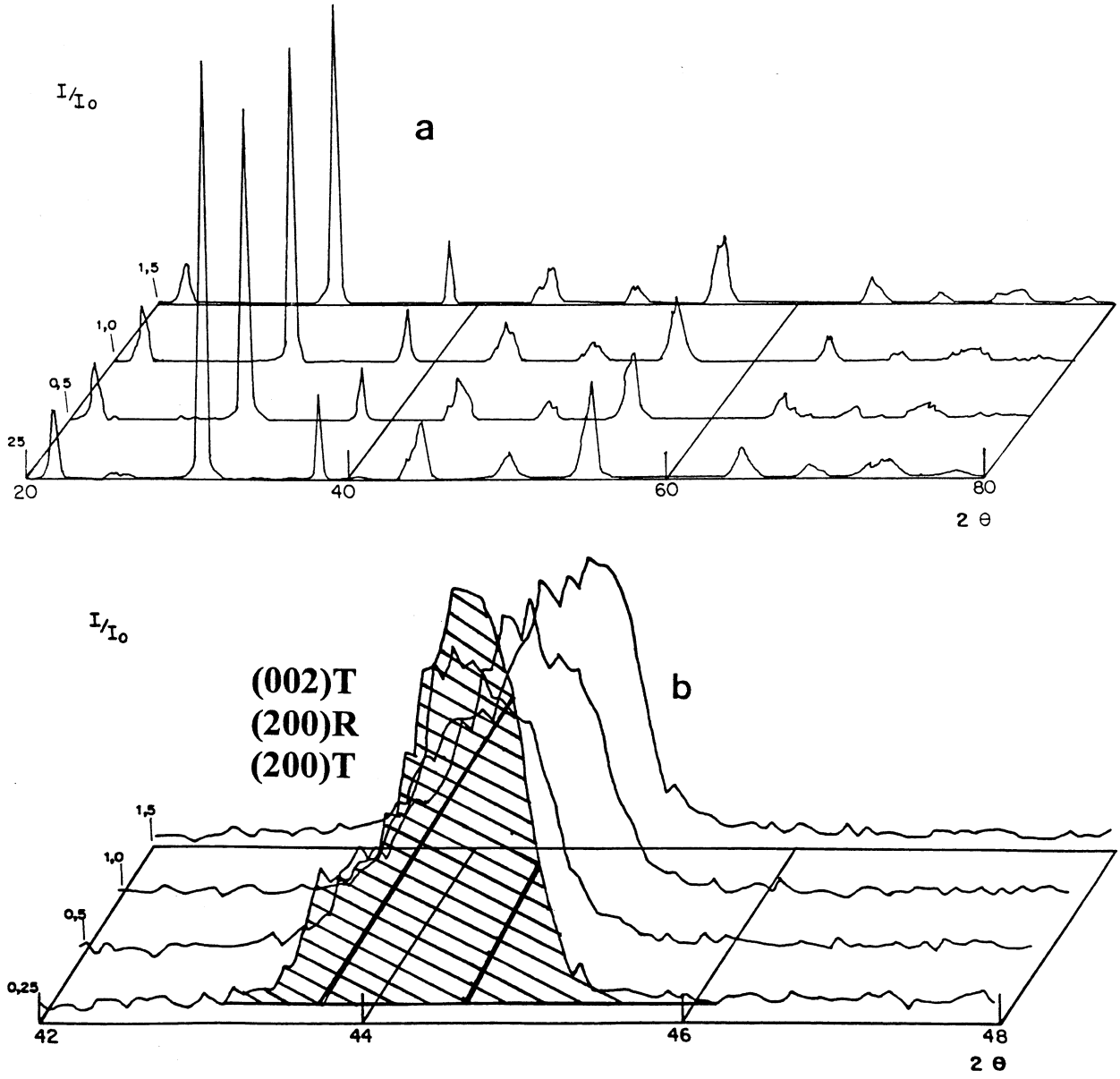

Fig. 1. X-ray diffraction pattern of sintered powder of strontium doped PZT. (a) Additions from 0.25 to 1.5 mol% of strontium, (b) deconvolution of peaks showed a coexistence between the tetragonal and rhombohedral phases. 1150°C/2 h.

bility of the tetragonal structure. Increases of remnant polarization, $\mathbf{P_R}$ compared with E_{latt} shows that the non-stable $\mathbf{F_R}$ could contribute to the polarization effect. Such data indicated that the tetragonal structure, $\mathbf{F_T}$ is not easily switched under the influence of an external electric field. An energetic stability of the $\mathbf{F_T}$ phase could not lead to an expansion of the ferroelectric domain walls due to a high tension state at the limit region of domain walls. An energetic unstability of the rhombohedral phase, $\mathbf{F_R}$, demonstrated that a moderate external electric field could cause a polarization effect in the bulk, with an increase of the volume of domain walls and a consequent increase of total polarization in the bulk. Despite the need of an $\mathbf{F_R}$ structure, under external electric fields, an unstable energy of the structure led to a strong dipole formation.

Experimental data, of the structure (Table 1), support the theoretical results showing that strontium in PZT led to decreases of the $(\mathbf{c}/\mathbf{a})_T$ ratio due to a decrease of the tetragonal unit cell volume, that caused formations of a stable local dipoles, $\mathbf{F_T}$ and lead to the appearance of an unstable $\mathbf{F_R}$ phase.

Tetragonal PZT with small $\mathbf{P_R}$ and very high $\mathbf{E_C}$ value showed an inversion tendency to the PZT-Sr solid solution formation. Such results are coherent with the calculated high stability of the $\mathbf{F_T}$ phase. Systematic addition of SrO in PZT decreased the unit cell volume of the tetragonal phase, and a deformed $\mathbf{F_R}$ phase, that

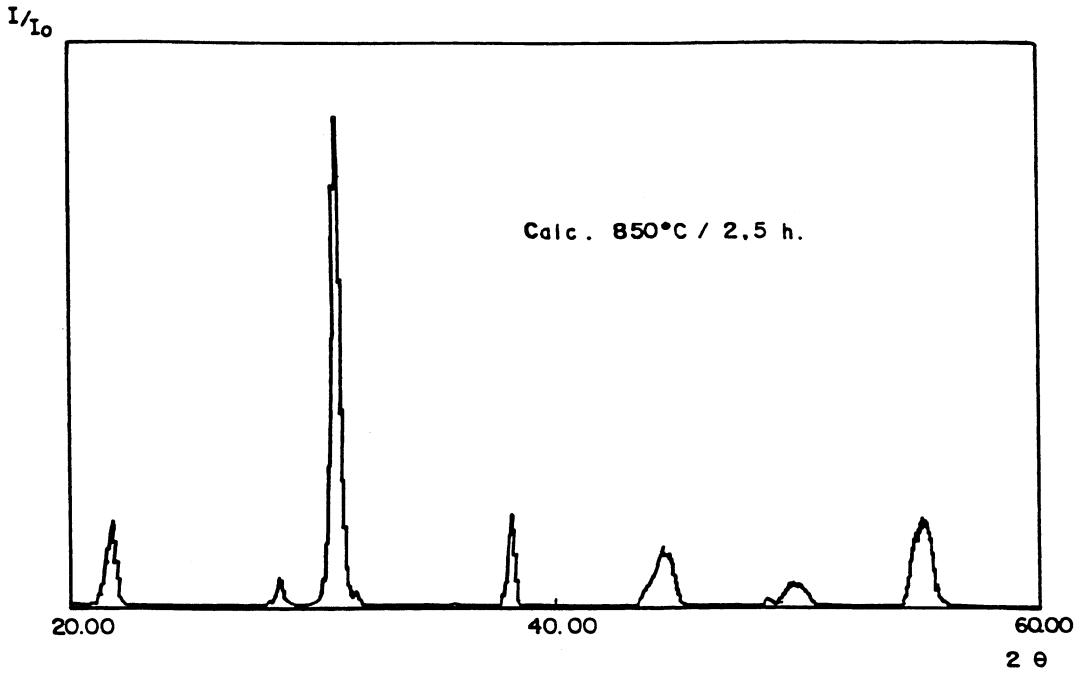

Fig. 2. X-ray diffraction pattern of PZT calcined at 850°C/2.5 h showing 100% of the tetragonal phase.

Table 2
$\mathbf{F}_T$, tetragonal phase's quantity, $(\mathbf{c}/\mathbf{a})_\mathbf{T}$, ratio between lattice parameters of tetragonal phase and $\mathbf{a}_R$, rhombohedral parameter lattice

	Additives (%)	$\mathbf{F_T}$ (%)	$(\mathbf{c}/\mathbf{a})_\mathbf{T}$	$\mathbf{a_R}$(Å)
PZT	0.00	100	1.0331	4.0695
	0.25	40	1.0197	4.0716
	0.50	43	1.0179	4.0784
	1.00	45	1.0186	4.0783
	1.50	47	1.0199	4.0760

Table 3
$\rho/\rho\mathbf{o}$, Relative density and $\mathbf{F_R}$ rhombohedral phase's quantity by different strontium concentrations

	$\rho/\rho\mathbf{o}$ (%)	$\mathbf{F_R}$ (%)
PZT	65	0
PZT-0.25	98	60
PZT-0.50	91	57
PZT-1.00	88	55
PZT-1.50	86	53

caused strong local dipoles under polarization, and increased the coercive field (Fig. 4). Alteration of chemical bonding, displacement and modification of characteristics of attraction–repulsion strengths occurred, high electric fields caused an increase of $\mathbf{E_C}$ value due to a stretching of chemical bonding of both $\mathbf{F_T}$ and $\mathbf{F_R}$ structures. The $\mathbf{P_R}/\mathbf{E_C}$ ratio showed a dislocation from square to rectangular hysteresis (reinforcement of the local polarization effect of the structure), with an increase of both $\mathbf{P_R}$ and $\mathbf{E_C}$ values when strontium is added.

Theoretical simulation of energy of Zr^{4+}/Ti^{4+} ions displacement in ABO_3 structure (Fig. 5a) shows an energy increase of tetragonal structure and an energy decrease of rhombohedral structure (Fig. 5b) with an increment of SrO. An increase of stability of the central ion of the rhombohedral phase caused an increase of the potential barrier of Zr/Ti ion displacement. A reverse tendency was observed for the tetragonal structure. Such results demonstrated that different interaction between atoms occurs. Due to this, alterations of the potential barrier for the ion displacement could occur as a consequence.

Comparisons of energies of tetragonal with rhombohedral structures showed that a high level of energy is necessary to move a central ion in the rhombohedral structure due to a likely deformation of unit cell. However, strong dipoles could be formed considering that a high stability of the tetragonal structure (lattice) leads to minor repulsion in the lattice. Due to this there are small potential barriers necessary for Zr/Ti ion dislocation.

Fig. 6 shows a coupling factor of about 0.53. Authors, like Kulcsar[17] and Lal et al.[27] studied strontium doped PZT and obtained $\mathbf{K_p} = 0.58$ and 0.47, respectively.

The increases of dielectric constant due to a high deformation energy of lattice led to alteration of the vibrational frequency, ν (optic phonons) by a relation, $\nu = \mathbf{1\text{-}2E}$, where $\mathbf{E}$ is the energy. This demonstrated that the fundamental frequencies, such as the resonance and anti-resonance, decreased with an increase of polarization energy of the system. Increases of the efficiency of the system have a direct effect on the increase of the material capacitance, $\mathbf{C_1}$ by a relation $\kappa^2 = \mathbf{C_1}/(\mathbf{C_1} + \mathbf{Co})$,

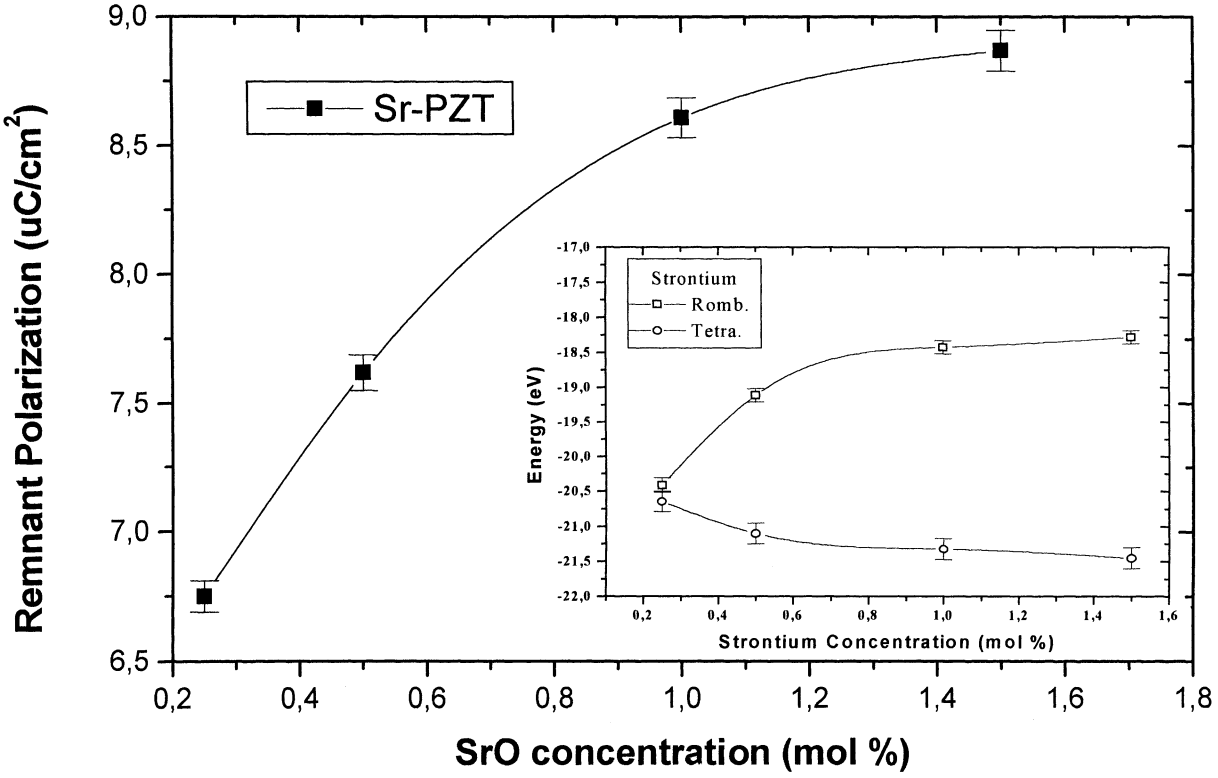

Fig. 3. Remnant polarization (P_R =[q(stored charge)/A(electrodes area)] against SrO concentration. Detail: as a comparision between theoretical and experimental data, a graphic of E_{latt} against SrO concentration is observed.

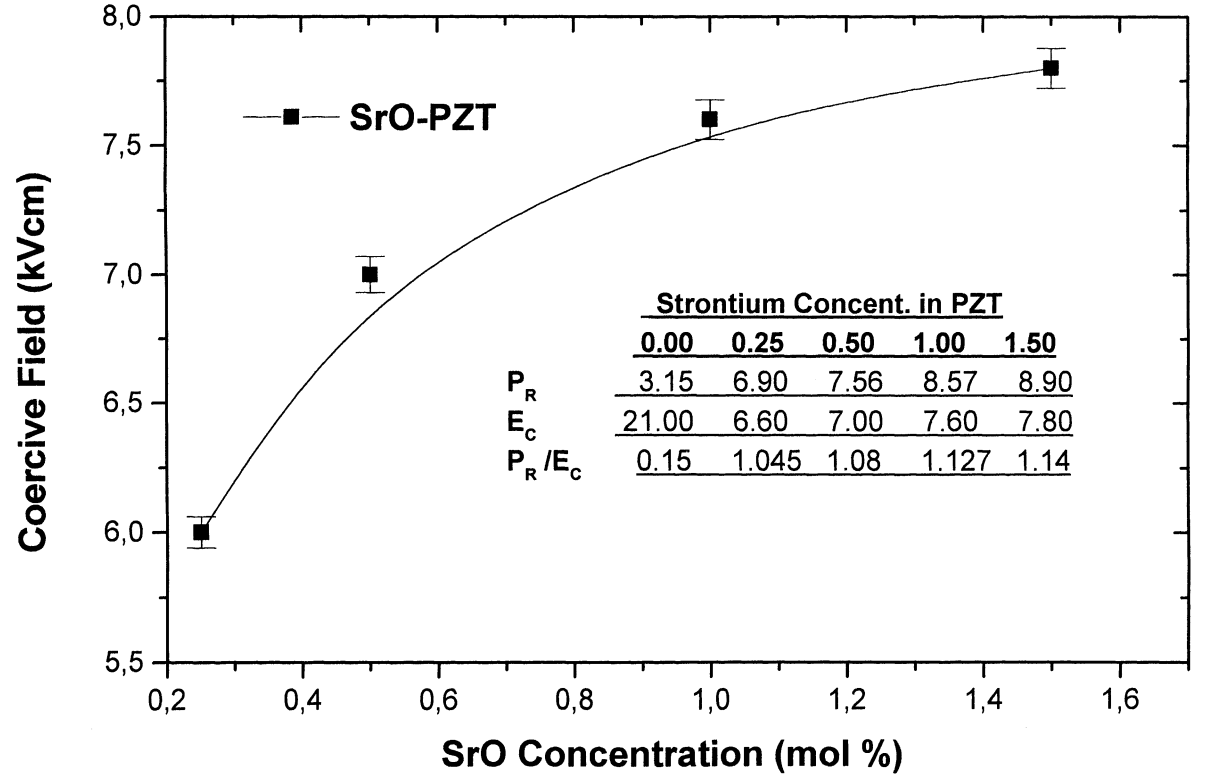

Fig. 4. Coercive field against the strontium concentration. Table: remnant polarization, $\mathbf{P_R}$, coercive field, $\mathbf{E_C}$, and $\mathbf{P_R/E_C}$ ratio.

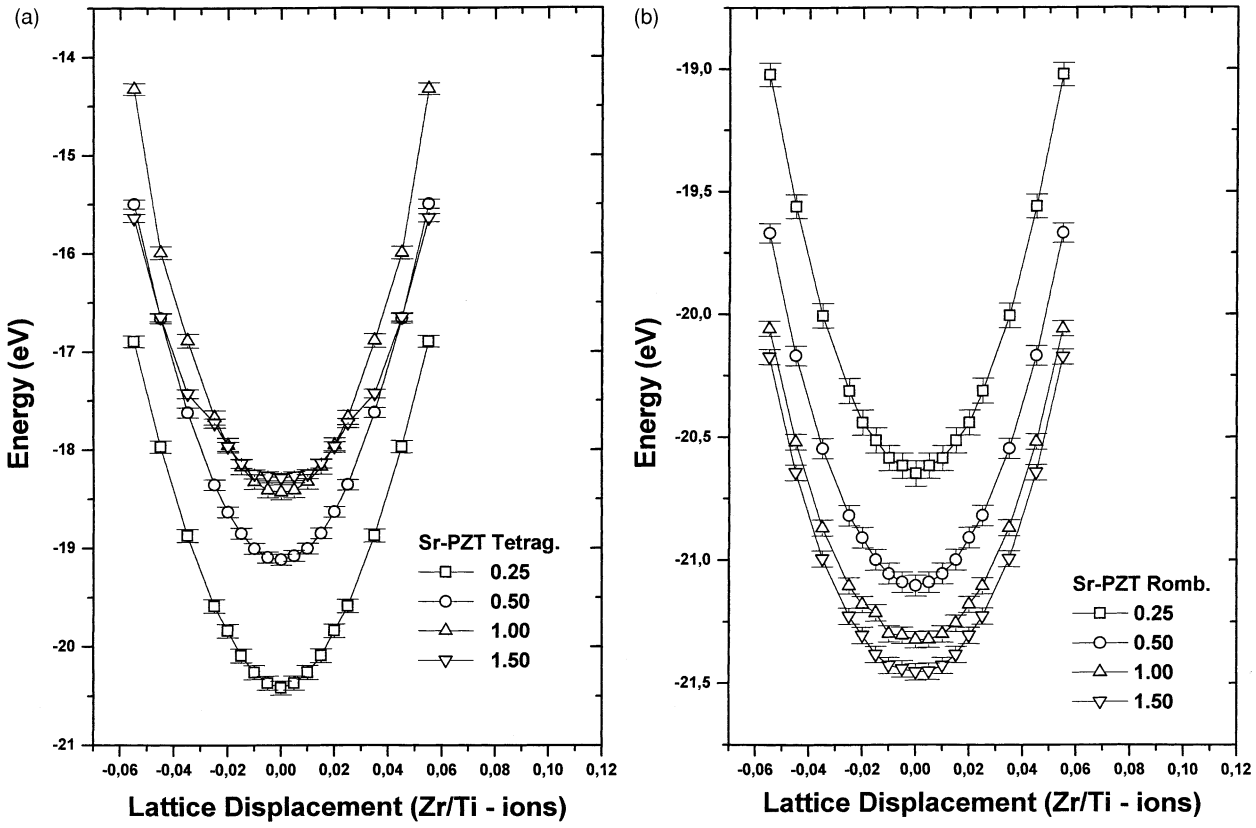

Fig. 5. Lattice displacement (Zr/Ti- Å) against the potential barrier of Zr/Ti ion dislocation, (a) Tetragonal structure; (b) rhombohedral structure.

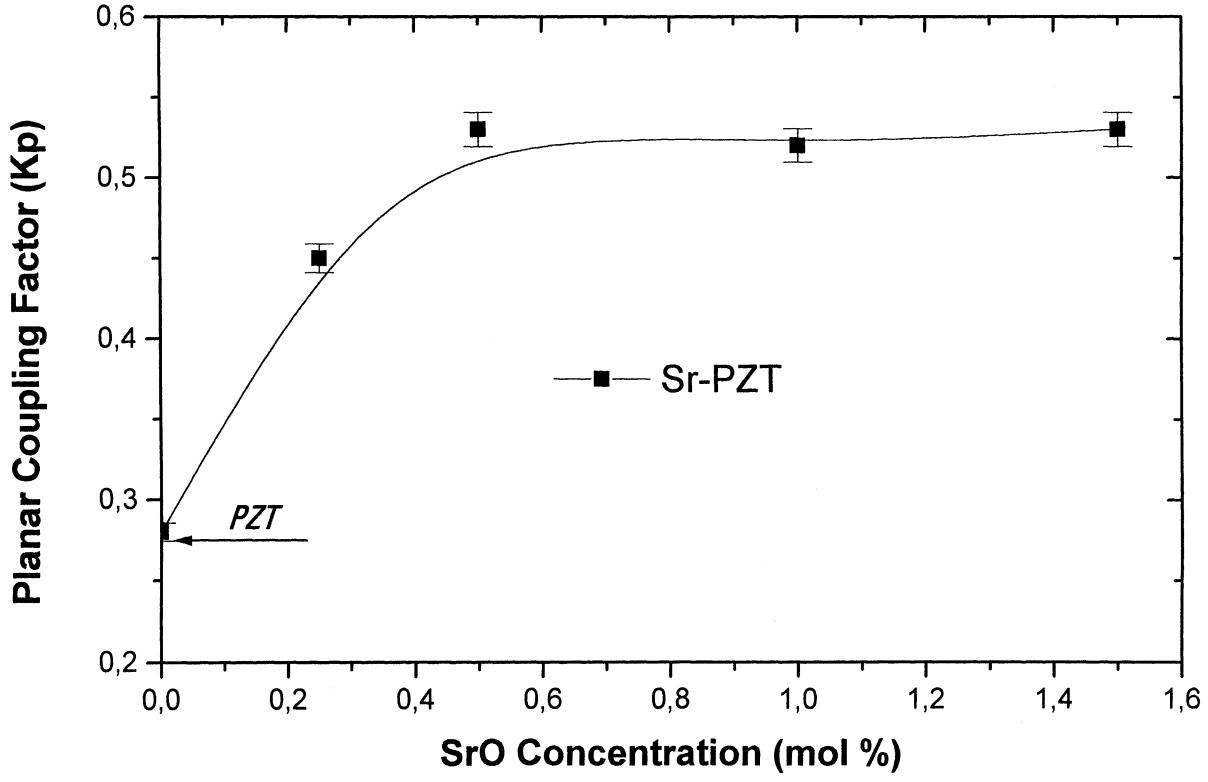

Fig. 6. Coupling factor against the strontium concentration.

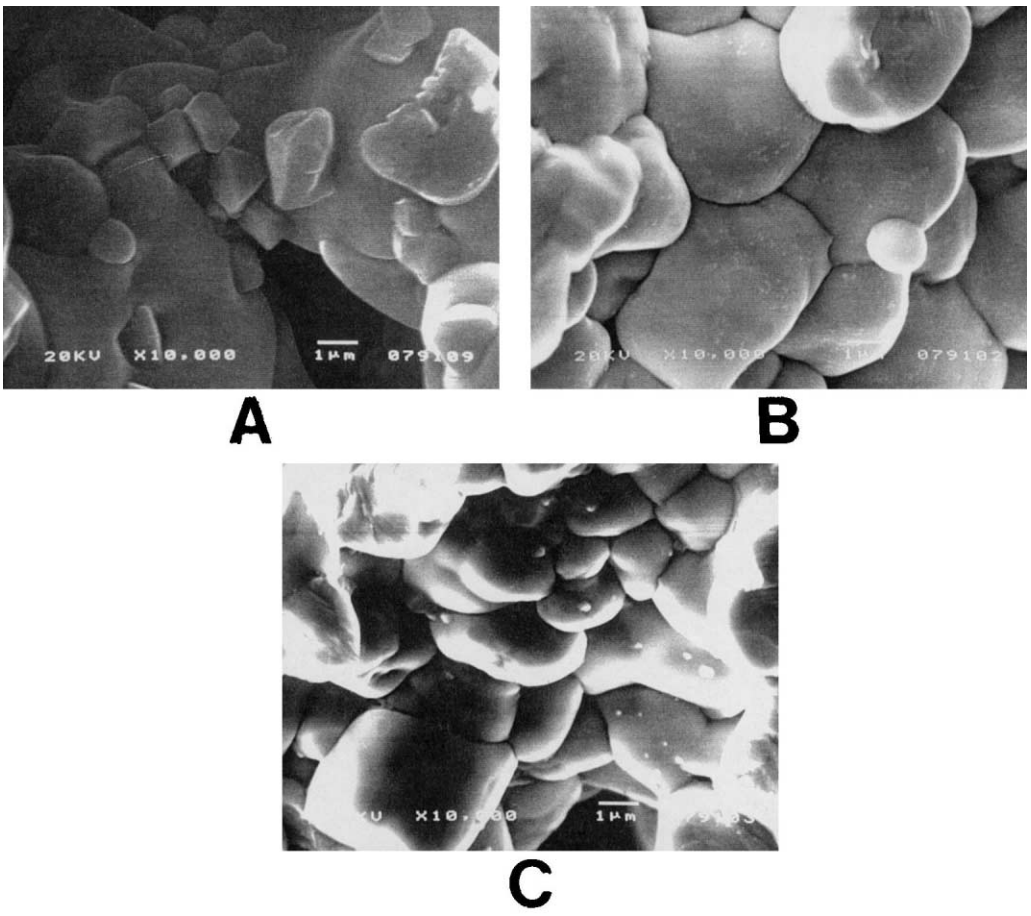

Fig. 7. Analysis by scanning electron microscopy SEM of the microstructure of strontium doped PZT sintered at 1150°C/3 h. (a) PZT; (b) 0.25%; (c) 1.00 mol% doped PZT.

where **Co** is the reference capacitance. Thus, the observed piezoelectric effect could be characterized by a stored electric charge in the grains of the microstructure.

4.3. Microstructural analysis

Analysis by scanning electron microscopy (SEM) of the PZT sintered powder shows abnormal grain sizes with high pore concentrations (Fig. 7a). Strontium additions in PZT (Fig. 7b and c) increased the microstructure homogeneity, decreased the pore size and showed densities of about 7.78 g/cm^3 (PZT) and 7.93 g/cm^3 (Sr-PZT, 0.25%). Addition of 0.25% of SrO concentration (Fig. 7b) shows a homogeneous grain size distribution and an optimization of microstructure.

PbO losses and an incomplete sintering process caused a decrease of the apparent density (Table 2) and led to a decrease of coupling between grains in the microstructure. The coupling factor is strongly dependent on coupling between grains of the microstructure, due to an increase of internal friction. High concentration defects, due to the pore presence, decreased the capacitance of the grains with a consequent decrease of polarization effect by a relation $\mathbf{P}=\mathbf{q}/\mathbf{A}$, where **q** is the stored charge and **A** is the transversal area. As a general effect, decreases of coupling factor occurred with a degradation of the transducer effect.

Theoretical analysis does not consider microstructure factors causing alterations of the dielectric and piezoelectric properties. Due to this, as a complement, a theoretical matrix does not prevent the presence of defects in the structure, they could occur as grain boundaries and vacancies and small errors. Considering the total effect of the polarization caused by a local dipole formation (ion dislocation) there was observed a large approximation between experimental and theoretical data.

5. Conclusion

Strontium additions in PZT led from a Zr rich region, which has tetragonal structure, to a Ti rich region, which has tetragonal and rhombohedral structures in the morphotropic phase boundary. The increases of remnant polarization and the coercive field supported the theoretical results which showed a decrease of lattice stability energy of the rhombohedral phase.

Simulations of the potential energy barrier of the PZT structure shows a reverse tendency between the tetragonal and rhombohedral phases when SrO is added. The strontium addition minimizes the energy of the rhombohedral phase.

Acknowledgements

The authors thank the CNPq for the financial support.

References

1. Cady, W. G., *Piezoelectricity*. McGraw Hill, New York. 1946 and Jaffe, B., Cook, W. R. and Jaffe, H., Piezoelectricity Ceramics. Academic Press, London, 1971.
2. Haertling, G. H., Piezoelectricity and electrooptic ceramics. In: *Ceramic Materials for Electronics*, ed. R. C. Buchanan. Marcel Dekker, New York, 1986.
3. Yamamoto, T., Optimum preparation methods for piezoelectric ceramics and their evaluation. *Ceram. Bull.,* 1992, **71**(6), 978–985.
4. Sawaguchi, E., Ferroelectricity and antiferroelectricity in the solid solution of $PbZrO_3$ and $PbTiO_3$. *J. Phys. Soc. Jpn.,* 1953, **8**, 615–629.
5. Benguigui, L., On the properties of PZT solid solutions: a replay to a comment. *Solid State Commun.,* 1986, **19**, 979–981.
6. Kanai, H., Furukawa, O., Abe, H. and Yamashita, Y., Dielectric properties of $Pb_{1-x}(Zr_{0.7}Ti_{0.3})O_3$ (x Ca, Sr, Ba) Ceramics. *J. Am. Ceram. Soc*., 1994, **77**, 26,20.
7. Lines, E. M. and Glass, A. M., *Principles and Applications of Ferroelectrics and Related Materials*. Claredon, Oxford, 1977.
8. Kakegawa, K., Mohri, J., Takahashi, T. H. and Shirasaki, S., Composition, fluctuation and properties of $Pb(Zr,Ti)O_3$. *Solid State Commun.,* 1977, **24**, 769.
9. Saha, S. K. and Agrawal, D. C., Composition fluctuations and their influence on the properties of lead zirconate titanate ceramics. *Am. Ceram. Soc. Bull.,* 1992, **71**(9), 1424–1428.
10. Haertling, G. H., Piezoelectric and electrooptic ceramics. In *Ceramic Materials for Electronics*, ed. R. Buchanan. Marcel Dekker, New York, 1986, pp. 168.
11. Isopov, V. A., Comments on the paper, X-ray study of the PZT solid solution near the morphotropic phase boundary in PZT solid solution. *Solid State Commun.,* 1975, **17**, 1331–1333.
12. Ari-Gur, P. and Benguigui, L., X-ray study of the PZT solid solution near the morphotropic phase transition. *Solid State Commun.,* 1974, **15**(6), 1077–1079.
13. Isopov, V. A., Characteristics of coexistence of tetragonal rhombohedral phases in piezoelectric ceramics based on $PbTiO_3$ and $PbZrO_3$. *Sov. Phys. Solid State,* 1976, **18**(4), 529–532.
14. Mabud, S. A., The morphotropic phase boundary in PZT solid solutions. *J. Appl. Cryst.,* 1980, **13**, 211–216.
15. Zhang, Q. M., Wang, H., Kim, N. and Cross, L. E., *J. Appl. Phys.,* 1994, **1**, 75.
16. Bernard, J., *Piezoelectric Ceramics*. Academic, London, 1971.
17. Kulcsar, F., Electromechanical properties of lead titanate zirconate ceramics with lead partially replaced by calcium or strontium. *J. Am. Ceram. Soc.,* 1959, **42**, 49–51.
18. Cerqueira, M., Nasar, R. S., Longo, E., Varela, J. A., Beltran, A., Llusar, R. and Andrés, J., Piezoelectric behaviour of PZT doped with calcium: a combined experimental and theoretical study. *J. Mater. Sci.,* 1997, **32**, 2381–2386.
19. Nasar, R. S., Cerqueira, M., Longo, E., Leite, E. R., Varela, J. A., Beltran, A. and Andrés, R., Experimental and theoretical study on piezoelectric behaviour of barium doped PZT. *J. Mater. Sci.,* 1999, **34**, 3659–3667.
20. Jaffe, B., Cook, W. R. and Jaffe, H., *Piezoelectric Ceramics*. Academic, New York, 1971.
21. Galasso, F. S., *Structure, Properties and Preparation of Perovskite-Type Compounds*. Pergamon, London, 1969.
22. Howard, C. J. and Hill, R. J., The polymorphs of zirconia phase abundance and crystal structure by Rietveld analysis of neutron and X-ray diffraction pattern. *J. Mater. Sci.,* 1991, **26**, 127–134.
23. Chandler, D., *Introduction to Statistical Mechanics*. Oxford University Press, Oxford, 1987.
24. Kirby, K. and Cooper, D., Electronic structure of atoms and molecules. In *Encyclopedia of Applied Physics*, Vol. 6, ed. E. G. L. Trigg. 45 VCH, New York, 1993, p. 45.
25. Atkins, P. W., *Physical Chemistry*, 5th edn, *Hartree-Fock Procedure*, Oxford, 1994, p. 446.
26. Kakegawa, K., Mohri, J., Takahashi, T., Yamamura, H. and Shirasaki, S., A compositional fluctuation and properties of Pb(Zr,Ti)03. *Solid State Commun.,* 1977, **24**, 769–772.
27. Lal, R. and Ramakrishan, R., Transition between tetragonal and rhombohedral phases of PZT ceramics prepared from spray-dried powders. *Br. Ceram. Trans.,* 1988, **87**, 99–102.